วิศวกรรมสารฉบับวิจัยและพัฒนา
Engineering Journal of Research and Development
วิศวกรรมสถานแห่งประเทศไทย ในพระบรมราชูปถัมภ์
The Engineering Institute of Thailand under H.M. The King's Patronage
ปีที่ 28 ฉบับที่ 2 เมษายน-มิถุนายน 2560
Volume 28 Issue 2 April-June 2017
Received 27 February 2017
Revised 2 May 2017
Accepted 9 May 2017

SIMULATION STUDY ON THE EFFECT OF INTERNAL PRESSURE IN ISRCTs COMPARED WITH FLUID MANDREL DRAWING METHOD

Tanit Tangsri
Department of Mechanical Engineering, Faculty of Engineering, Thonburi University, Bangkok, Thailand

ABSTRACT

The objective of this research paper is to identify the effect of internal pressure deformation behaviours of ribbed spiral angle and the ribbed cross-sectional profile of ultra-small inner spiral ribbed copper tubes (ISRCTs) which have high quality and efficiency in transferring heat. Modelling and simulation techniques were performed by using commercial Abaqus software to observe whether the surface profiles of the ISRCTs was increased or decreased with various internal pressures (pressure gauge: 0, 1, 2 and 3 bar) on the tube drawing. The effect of any parameters cannot be found by experimental method. Twelve multi-passes drawing with internal pressures 0, 1, 2 and 3 bar was summarised and compared to the fluid mandrel drawing in similar to 1-3 multi-pass drawing, 4-6 multi-pass drawing, 7-9 multi-pass drawing, and 10-12 multi-pass drawing respectively. In various internal pressures, the FEM simulation approach was used to analyse the changes of ten parameters: von Mises stress, wall thickness, ribbed base width, ribbed tip width, ribbed base gap, ribbed tip gap, ribbed height, ribbed pitch, axial displacement and ribbed spiral angle. The results will be very valuable for researchers and well engineers for future design of ultra-small ISRCT to improve the quality and efficiency of heat transfer.

KEYWORDS: Ultra-small inner spiral ribbed copper tube, Pressure inside ISRCT, Finite element method, Fluid mandrel drawing.

1. Introduction

The development of ultra-small ISRCT with high-quality heat transfer using tube sinking and water, oil, and wax as mandrels in drawing were taken. It was found that, the tube sinking was unsuitable for drawing the ultra-small inner spiral ribbed copper tubes because of large wall thickness ratio has very small ribbed spiral angle inside the tubes. The wax mandrel drawing is the best of the four methods in the production of ultra-small inner spiral ribbed copper tubes with high-quality heat transfer; however, this method is unsuitable for fabrication of long ultra-small tubes because of the difficulty in removing wax from the tubes after drawing. The fluid mandrel drawing is more efficient for fabrication of long ultra-small inner spiral ribbed copper tubes with high-quality heat transfer because of the ease removal of the fluid from the tubes after drawing. The wall thickness of the tubes after drawing using fluid mandrels, i.e. water and oil, is slightly different depending on the type of fluid filled inside the tube. Nevertheless, the wall thickness of the tubes using either drawing method is almost identical to that of the mother tube. The

cross section of the copper tube decreases with each drawing but at a slower rate than the tube sinking method. The fluid mandrel drawing using water is the most appropriate for fabrication of the tubes because of the ease removal of the water from inside of the tube than oil [1]. The fluid mandrel drawing ISRCTs methods and results are shown in Figure 1.

In this experiment, seamless inner spiral ribbed copper tubes were used as specimens (5.00 mm outside diameter, 3.71 mm inside diameter, 0.364 mm wall thickness, 0.28 mm rib height, 0.33 mm rib base width, 0.175 mm rib tip width, and 45 ribs). The seamless inner spiral ribbed copper tubes were cut longitudinally, and the cut tubes were found to have 38° spiral angle and 0.393 mm rib pitch.

The tube sinking includes axial stress, radial stress, and hoop stress. The compressive stress will occur at the tube wall. But it may change to the tensile stress within the area of the rib. Compressive stress is the fact value that distributed within the range of the radius of the tube wall and diffused within the area of the rib inside the tube. It will have the same value of what occurs in the area of the wall and rapidly expanding in the area of the rib. While using tube sinking drawing method, the inner spiral rib has changed a lot, consisted of the thickness of the tube wall, which increased repeatedly and continuously. But ribbed height (the height of the rib), ribbed base width (the width of the ribbed base), ribbed tip width (the width at the top of the rib), ribbed pitch (Pitch direction of the rib) and ribbed spiral angle are decreased dramatically [2]. While using tube sinking drawing method. During using tube sinking drawing, the inner spiral rib has changed a lot including the thickness of the tube wall, which increased repeatedly and continuously. But the ribbed height, ribbed base width, ribbed tip width, ribbed pitch, and ribbed spiral angle was decreased after that the spiral angle of the ribbed [3].

The drawing stress was derived from the axial stress, radial stress and hoop stress. In fabricating ISRCTs, the ratio of drawing stress to yield stress (σ/σ_y)=1.00 was determined by the outside diameter. This was accurate standard size or expected design and could be used in industrial manufacturing. The height of the ribbing was reduced with compressive strain in the circumferential direction, and there was no pressure inside the tube for the deformation resistance. If the wall thickness plus the rib height divided by the diameter was equal to 0.50 [$(t_w+h_r)/D=0.50$], then the tube was closed at the end and could not transmit any fluid. If the ribbed base width multiplied by the total ribbing inside the inner copper tube divided by the length of the ribbed base circumference of the ribbed base width of the ISRCT was equal to 1.00 [$w_{rb}/(\pi d_{rb}/n)=1.00$], then the heat transfers at the ribbed gap on the ribbed base were inefficient and showed features similar to conventional tubing. If the ribbed tip width multiplied by the total ribbing inside the copper tube, divided by the length of the ribbed tip, was equal to 1.00 [$w_{rt}/(\pi d_{rt}/n)=1.00$], then the gap between the ribs vanished and heat transfers were the same as conventional tube. The deformation of the ribbed base was more than at the ribbed tip; ψ^o reduced continuously and in a negative way. If ψ^o was close to zero, then the heat transfer would have the same effect as a straight ribbed tube [4]. The drawing force increased as the coefficient of friction values increased. Because of limitations of the lubricants available and tool material, this value currently 0.02. The tube sinking method is a process which arises from stress, including axial stress, radial stress and hoop stress.

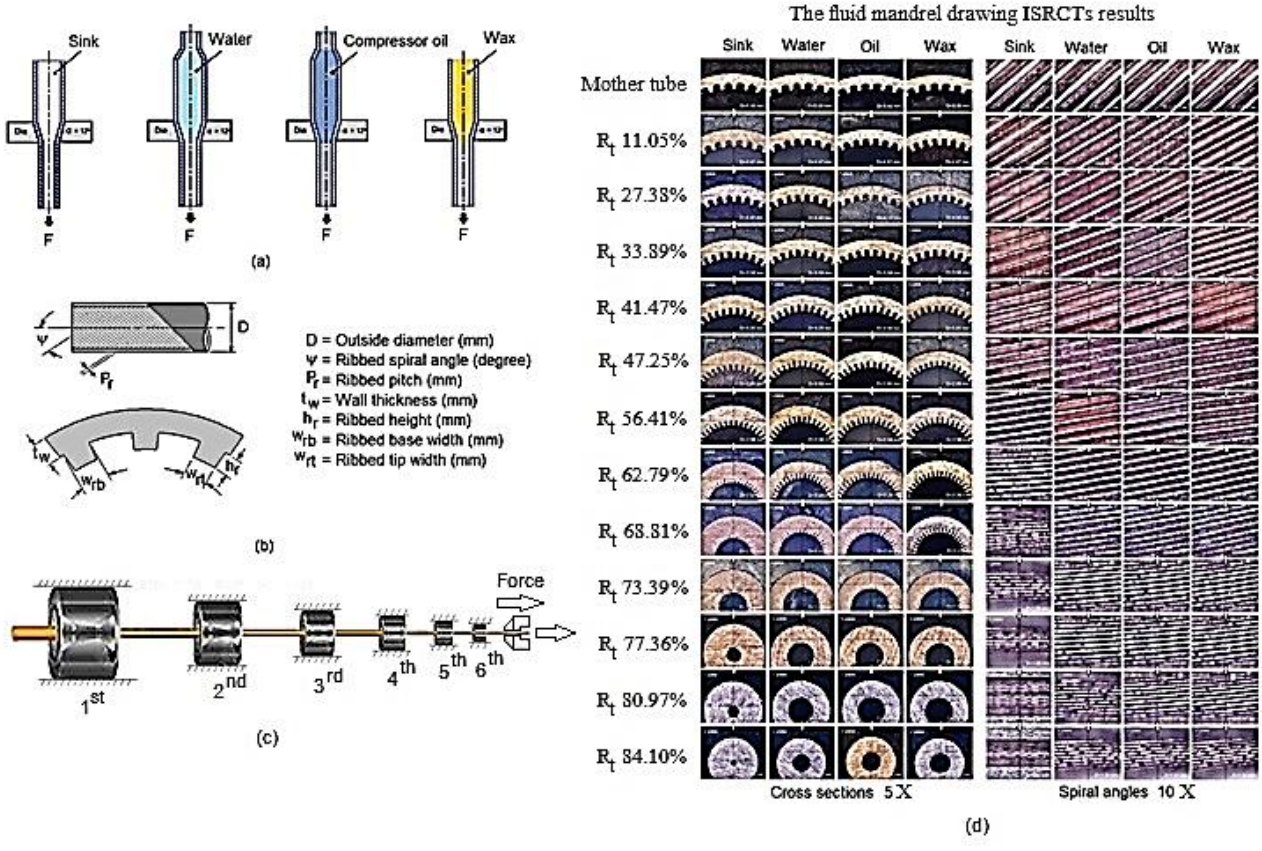

Figure 1 **(a)** The four drawing methods. *F* drawing force (N), α approach semicone angle of die (die half-angle, in degrees). **(b)** The cross-sectional and longitudinal drawings of the inner spiral ribbed copper tube. **(c)** The multi-passes drawing methods (d) The cross sections. 5X and the spiral angles. 10X of ribs using the four drawing methods [1].

The stress increases in the ribbed wall and rapidly expands into the ribbed area regions. The von Mises stress after 12 multi-pass drawings was different for each locality. The stress was greatest at the base of the ribbed regions, intermediate at the surface on the outer layer regions and minimum at the middle of the wall thickness and at the tip of the ribbed regions respectively. The expansion of the effective strain occurred as growth assimilation within the limits of the ISRCT boundary. During the tube sinking, the ISRCT altered greatly and the von Mises stress, wall thickness and axial displacement increased repeatedly and continuously. The ribbed base width, ribbed tip width, ribbed base gap, ribbed tip gap, ribbed height, ribbed pitch and ribbed spiral angle however decreased after 12 multi-pass drawings of the ISRCT. The results of the experimental and 3D FEM simulation were coincident with data from the tube sinking method. The analysis of the ten parameters varied in the ultra-small ISRCT, the most appropriate total reduction area must not exceed 68.81 % because the gaps disappear and flute and lug marks appear on the side of the ribbed area. These results can be used to predict the final precision diameter of the ISRCT for manufacturing [5].

2. Theory

The standard equation of reduction of area (%) is as follows:

$$RA = \frac{A_b - A_f}{A_b} \times 100 \ (\%) \tag{1}$$

where RA = reduction of area (%); A_b = initial area (mm^2); A_f = final area (mm^2) [6]. The cross-sectional reduction of area of the ISRCT is defined by:

$$A = A_w + A_r \tag{2}$$

$$A = \frac{\pi}{4}\left(D_0^2 - d_w^2\right) + \left[\left\{\frac{1}{2}\left(w_{rb} + w_{rt}\right)h_r\right\} \times 45\right] \tag{3}$$

Where A = cross-sectional area (mm^2), A_w = cross-sectional area of the wall (mm^2), A_r = cross-sectional area of the ribbing (mm^2), D_0 = outer diameter (mm), $D_w = D_0 - 2t_w$ inner diameter (mm), w_{rb} = ribbed base width (mm), w_{rt} = ribbed tip width (mm), h_r = ribbed height (mm) and 45 is the number of ribs in the mother tube. The total reduction of area (%) is as follows: where R_t the summation reduction of area (%) [4].

$$R_t = \sum\left(RA_1 + RA_2 + RA_3 \ldots\ldots\ldots\ldots RA_{final}\right) (\%) \tag{4}$$

The stresses involved in tube sinking can be analysed by the method of Sachs and Baldwin [7] on the assumption that the wall thickness of tube remains constant. The equation of the drawing stress at the die exit was analogous to that describing the drawing stress in the cross-sectional area of the tube was related to the middle radius *r* and the wall thickness *h* by $A \approx 2\pi rh$ [6].

$$\sigma_{xa} = \sigma_0'' \frac{1+B}{B}\left[1 - \left(\frac{A_f}{A_b}\right)^B\right] \tag{5}$$

Where *B* is given by:

$$B = \mu \cot \alpha \tag{6}$$

And

μ = Coefficient of friction between tube and die wall.

α = Half-angle of die.

The yield stress was taken equal to 1.1 for the complex stresses in tube sinking. A more complete analysis of tube sinking has been given by Swift [6]. The drawing stress is derived from axial stress, radial stress and hoop stress. The tube sinking yielded the lowest drawing stress used in the manufacture of inner spiral ribbed copper tube [1].

3. FEM simulation methods

For this FEM simulation model, seamless inner spiral ribbed copper tubes (ISRCTs) were used as specimens. The tube drawing process with ISRCT used as specimens with dimensions of 5.00 mm outside diameter, 3.90 mm inside diameter, 0.370 mm wall thickness, 0.18 mm rib height, 0.18 mm rib base width, 0.10 mm rib tip width, 34.20° rib spiral angle and 0.27 mm rib pitch for 45 ribs. Coefficient of friction between tube and die wall (μ=0.02). The tungsten die was modelled as a rigid body, the die half-angle was 12° (α=12°) and the drawing speed kept stable at 150 mm/s. The cross-section area of reduction per pass (RA/P) was kept between 7 and 25 %. The cross-section of the ISRCT is shown in Figure 2, and the parameters of the specimen mother tube are listed in Table 1.

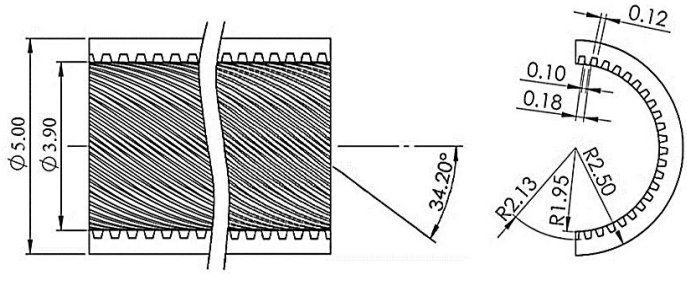

Figure 2 Cross-section of the ISRCT

Table 1 Material properties and drawing conditions used (mother tube)

Young's modulus, E (GPa)	110
Buck modulus, k (GPa)	114.58
Shear modulus, G (GPa)	41.045
Tangent modulus, E_t (GPa)	1
Yield stress, σ_y (MPa)	150
Ultimate stress, σ_u (MPa)	250
Poisson's ratio, ν	0.34
Die half-angle, α (degrees)	12
Coefficient of friction, μ	0.02
Density, ρ (kg/m^3)	8300

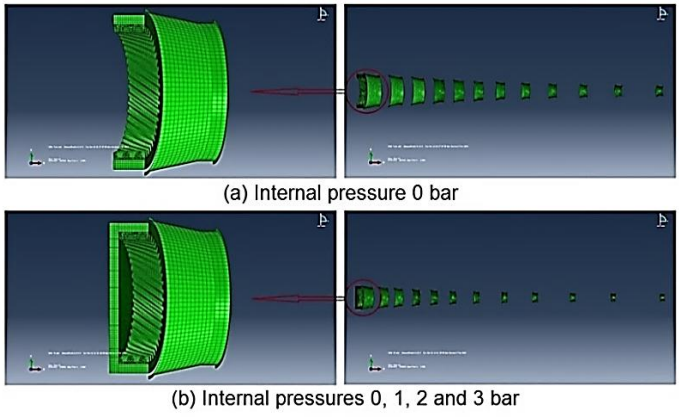

Figure 3 3D models of ISRCT and dies used for simulation

A 3D FEM uses a numerical analysis technique for approximating solutions for a variety of engineering problems. FEM originated as a method of stress analysis, and the procedure produces many simultaneous algebraic equations which are generated and solved using computer techniques. It transforms a physical system with an infinite number of unknowns into a system with a finite number of variables. 3D models of ISRCT and dies were generated using key points, lines and areas. The cross-section was then revolved about the x-axis to obtain the quarter model. The cross-sections and longitudinal sections of the ISRCT simulation models used the axis of force in the tube multi-drawing. 3D models of ISRCT and dies used for simulation are shown in Figure 3.

Finite element analysis of tubular expansion was performed using Abaqus software. Mapped fields can only be used in models in which supported element types are used in the mesh. The most commonly used elements are supported, including shells. Supported element classes are according to the topology of the representative element type, shape, number of nodes and number of integration points. In this simulation, the total elements of ISRCT are well-adapted for 3D with 104,814 solid element contacts. There are two main components, C3D4 4-node linear tetrahedron with 84,074 solid element inertia loads on the ribbed region. For stress/displacement analyses, the first-order tetrahedral element C3D4 is a constant stress tetrahedron, which should be avoided as much as possible as the element exhibits slow convergence with mesh refinement. This element provides accurate results only in general cases with very fine meshing. Therefore, C3D4 is recommended only for filling in regions of low stress gradient in meshes of elements. The wall of the tube has 20,740 solid elements of C3D8R 8-node linear brick and reduced integration with hourglass control. This is a well-adapted element for 3D contact and for forming simulations. Abaqus/Explicit offers two alternative kinematic formulations for the C3D8R solid element that can reduce the computational cost. The total elements of die are 1683 quadrilateral linear, R3D4 4-node 3D bilinear rigid quadrilateral. R3D4 elements can specify the thickness of the element if no thickness is given. The continuum, structural and rigid element types can be included and the respective node types generated in the rigid body. When connector elements are included in the rigid body, the type of generated nodes depends on whether the rotational degrees of freedom are active for their connection type. If connector elements that

activate the material flow degree of freedom at nodes are included in the rigid body, the material and flow through the rigid body as that degree of freedom are constrained by the motion of the rigid body. The supported representative elements are shown in Figure 4.

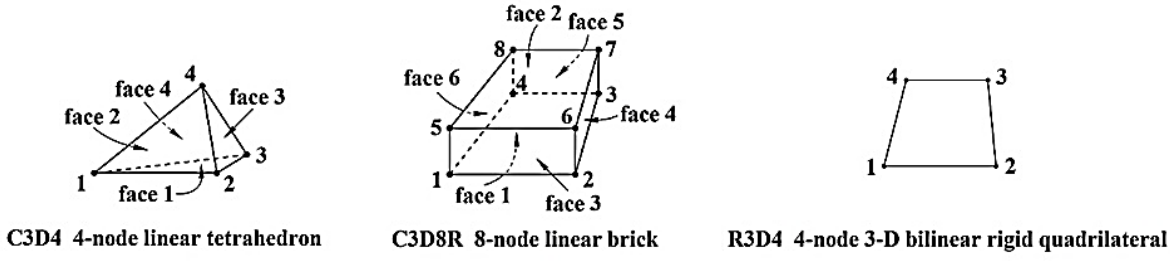

Figure 4 3D node structural solid element

Meshing of the ISRCT and die for the tube sinking method was done by using a 3D node structural solid element. The material had nonlinear characteristics, shown in Figure 5a. The analysis concerned the contacts taking place between the inner surface of the die and the outer surface of the ISRCT. A contact pair was generated using the contact wizard and a friction contact with coefficient of friction 0.02 was modelled. Various lubricants were also incorporated in the modelling by inputting values of the coefficient of friction. The contact pair between the ISRCT and die is shown in Figure 5b. In the simulation, the die was fixed, and the tube moved past the die along the x-direction. Boundary conditions were applied on the nodes. The number of unknowns in the global force vector produced more global displacement vector matrices than equations. After applying boundary conditions, the number of unknowns reduced to equal to or less than the number of equations. The boundary conditions of the ISRCT and die are shown in Figure 5c. The material used for the ISRCT in the tube sinking had a modulus of elasticity of 110,000 N/mm^2 and Poisson's ratio 0.34. There was a nonlinear type of contact analysis between the die inner and the ISRCT outer surfaces. Thus, it became necessary to introduce the nonlinear nature of the material in the analysis. Figure 5d shows the nonlinear behaviour of the ISRCT material as a stress–strain diagram. In the analysis, the part under study is the ISRCT and not the die. The die material is assumed to have a very high value of the modulus of elasticity at 2.1×109 N/mm^2 and a Poisson's ratio of 0.3

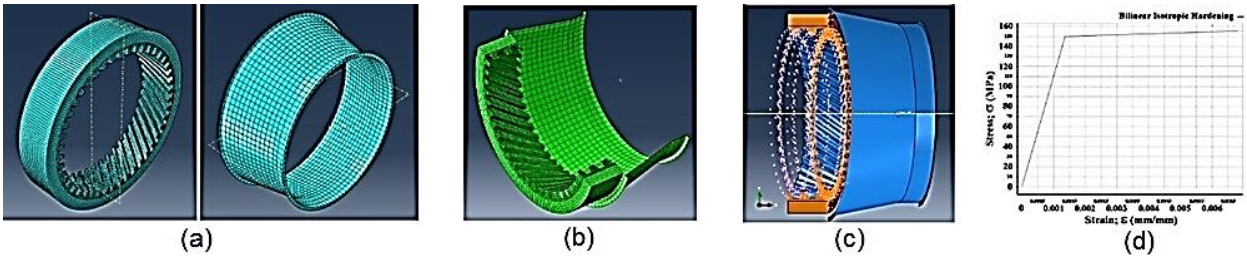

Figure 5 Simulation model. **a** Meshed model ISRCT and die. **b** Contact pair between the ISRCT and die. **c** Boundary conditions for the ISRCT and die. **d** Stress–strain curve of the ISRCT

The cross sections and the spiral angles of the ribbing using tube drawing with various internal pressures (pressure gauge: 0, 1, 2 and 3 bar) on tube drawing and compared to the fluid mandrel drawing [1]. From the results, the internal pressure 0 bar (no pressure inside ISRCT) the changes of ribbed cross-sectional profile was similar to 1-3 multi-pass drawing of fluid mandrel drawing, and the internal pressure 1, 2 bar the changes of ribbed cross-sectional profile was similar to 4-6, 7-9 multi-pass drawing of fluid mandrel drawing, and likewise the internal pressure 3 bar the changes of ribbed cross-sectional profile was similar to 10-12 multi-pass drawing of fluid mandrel drawing respectively. The drawing stresses as von Mises distributions in the tube drawing with various internal pressures process were calculated using commercial Abaqus software. The experimental of fluid mandrel and simulation tests as well as some other drawing variants, with different profile parameters, were evaluated numerically. The total reduction of area was decreased for each successive tube specimen; R_t was 11.05 % for the first tube specimen, 27.38 % for the second and so on until R_t was 84.10 % for the drawing. The percentage of the area was increased, and the concave profiles of the ISRCTs were taken into consideration. After of total reduction of the area using a half-angle 12° die (α=12°), the deformation behaviour of the ISRCT with various internal pressures on tube drawing is shown in Figure 6.

From the aforementioned figure, as the outer diameters were reduced, the inner spiral ribs and pitches contracted while the inner surface became uneven. The contraction rates were different for various internal pressures inside the tubes, resulting in unequal rates of increase of wall thickness, axial displacement and von Mises stress. Contrary to the rise of the previous parameters, rib base width, rib tip width, rib base gap, rib tip gap, rib height, rib pitch and rib spiral angel decreased with each pass. The strain distribution of the rib was not uniform from the rib base to the rib tip, and the strain was greatest at the tip. The deformation at the rib base was more severe than at the rib tip, while the spiral rib angle decreased with each pass. The tube sinking method (0 bar) showed the greatest change in all of the aforementioned parameters, compared with the tube drawing methods for various internal pressures inside the tubes (1 bar, 2 bar and 3 bar) all of the aforementioned parameters had less changes. The cross-sections and spiral angles of the ribs tube drawing with various internal pressures by 3D FEM is shown in Figure 6.

The drawing stresses of each internal pressure inside the tubes are derived from axial stress, radial stress, and hoop stress. Axial stress is the tensile stress on the wall and the ribbed area of tube, radial stress is the compressive stress in the tube wall zone, and hoop stress is the stress caused by the pressure inside the compressive stress. The results of FEM analysis of von Mises stress waves are shown as 12 multi-pass drawings, drawing process were calculated by using commercial Abaqus software. Meshing of the ISRCT and die for various internal pressures inside the tubes was done by using a 3D node structural solid element. In this case, the colour grey was selected for elements with no results. The die elements appear grey because the die is a rigid surface for which no stress resulted exist. The results of the ISRCT specimens are available in the output database file created by the 12 steps of multi-pass drawing by the optimisation process different for various internal pressures inside the tubes before and after on the 1–12-step multi-pass process are shown in Figure 7a.An elastic–plastic material ISRCT was used in the FEM software with an isotropic hardening law. The von Mises criterion with radial return was used for the flow stress and the

material was considered strain rate independent. Von Mises stress and FE simulation time were different for various internal pressures inside the tubes configuration at any point as shown in Figure 7b.

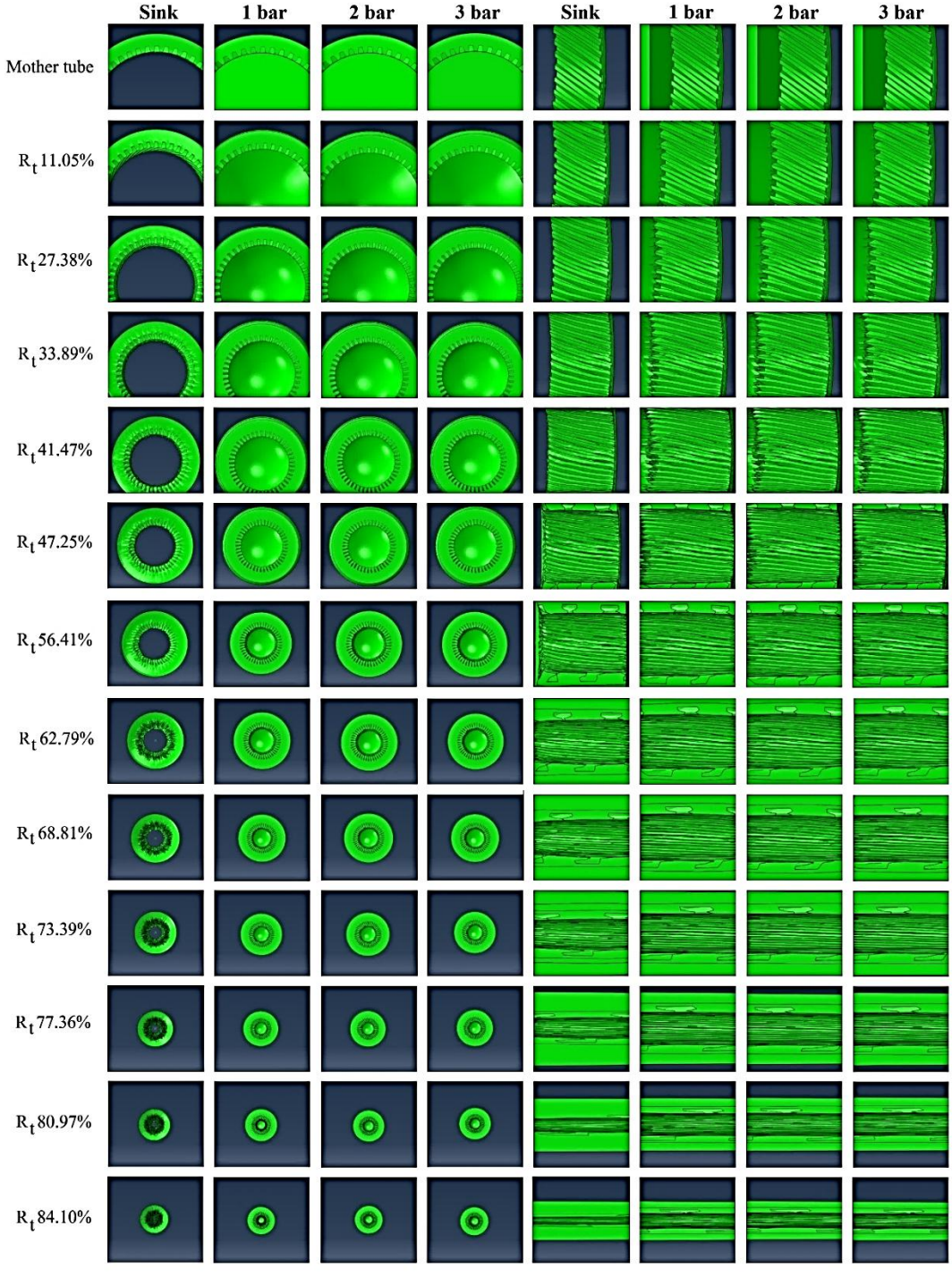

Figure 6 The cross-sections 5X and the spiral angles 10X of the ribs tube drawing with various internal pressures by 3D FEM

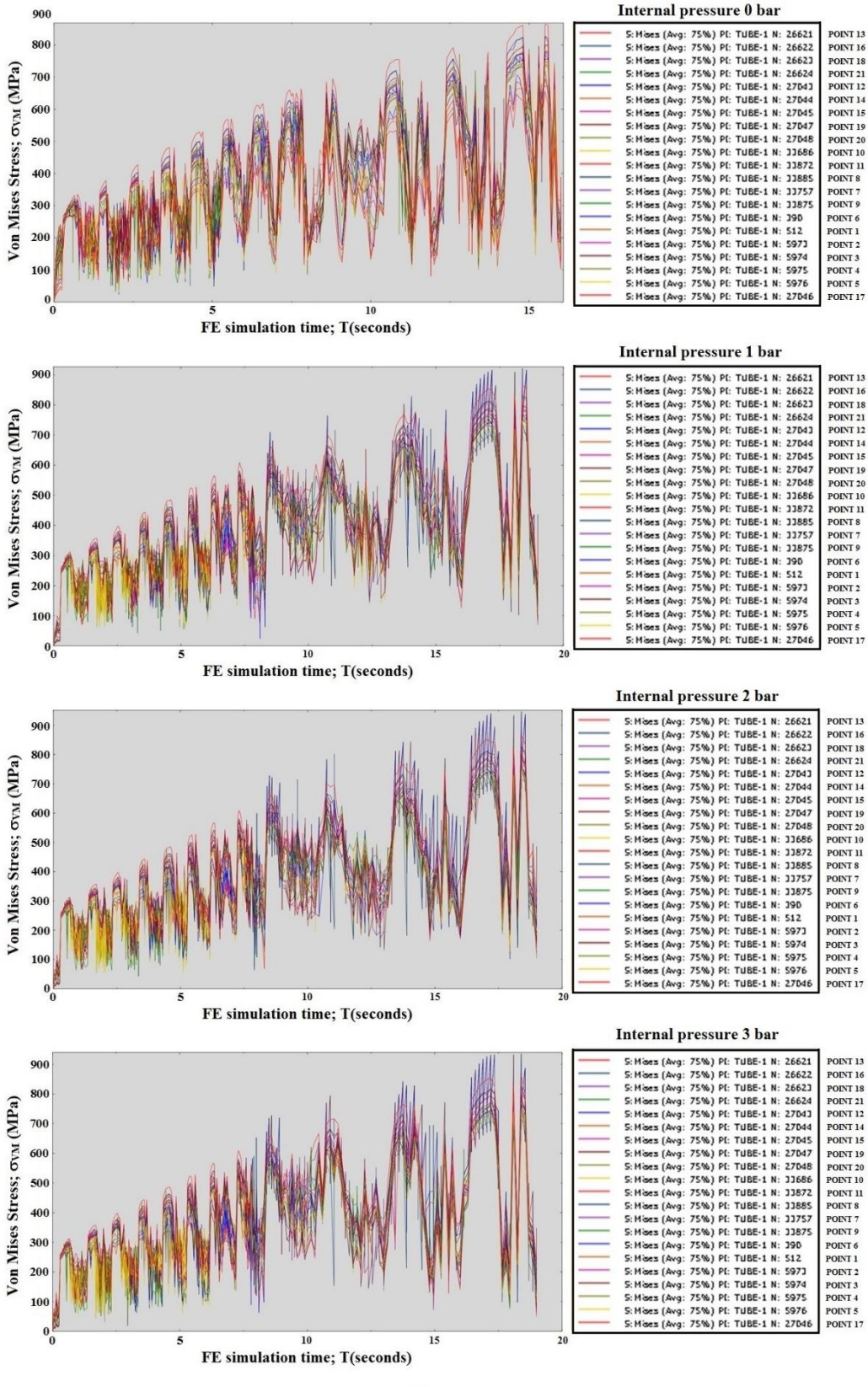
Internal pressure 0 bar
Internal pressure 1 bar
Internal pressure 2 bar
Internal pressure 3 bar
Von Mises Stress; σVM (MPa)
FE simulation time; T(seconds)
S: Mises (Avg: 75%) PI: TUBE-1 N: 26621 POINT 13
S: Mises (Avg: 75%) PI: TUBE-1 N: 26622 POINT 16
S: Mises (Avg: 75%) PI: TUBE-1 N: 26623 POINT 18
S: Mises (Avg: 75%) PI: TUBE-1 N: 26624 POINT 21
S: Mises (Avg: 75%) PI: TUBE-1 N: 27043 POINT 12
S: Mises (Avg: 75%) PI: TUBE-1 N: 27044 POINT 14
S: Mises (Avg: 75%) PI: TUBE-1 N: 27045 POINT 15
S: Mises (Avg: 75%) PI: TUBE-1 N: 27047 POINT 19
S: Mises (Avg: 75%) PI: TUBE-1 N: 27048 POINT 20
S: Mises (Avg: 75%) PI: TUBE-1 N: 33686 POINT 10
S: Mises (Avg: 75%) PI: TUBE-1 N: 33872 POINT 11
S: Mises (Avg: 75%) PI: TUBE-1 N: 33885 POINT 8
S: Mises (Avg: 75%) PI: TUBE-1 N: 33757 POINT 7
S: Mises (Avg: 75%) PI: TUBE-1 N: 33875 POINT 9
S: Mises (Avg: 75%) PI: TUBE-1 N: 390 POINT 6
S: Mises (Avg: 75%) PI: TUBE-1 N: 512 POINT 1
S: Mises (Avg: 75%) PI: TUBE-1 N: 5973 POINT 2
S: Mises (Avg: 75%) PI: TUBE-1 N: 5974 POINT 3
S: Mises (Avg: 75%) PI: TUBE-1 N: 5975 POINT 4
S: Mises (Avg: 75%) PI: TUBE-1 N: 5976 POINT 5
S: Mises (Avg: 75%) PI: TUBE-1 N: 27046 POINT 17

(a)

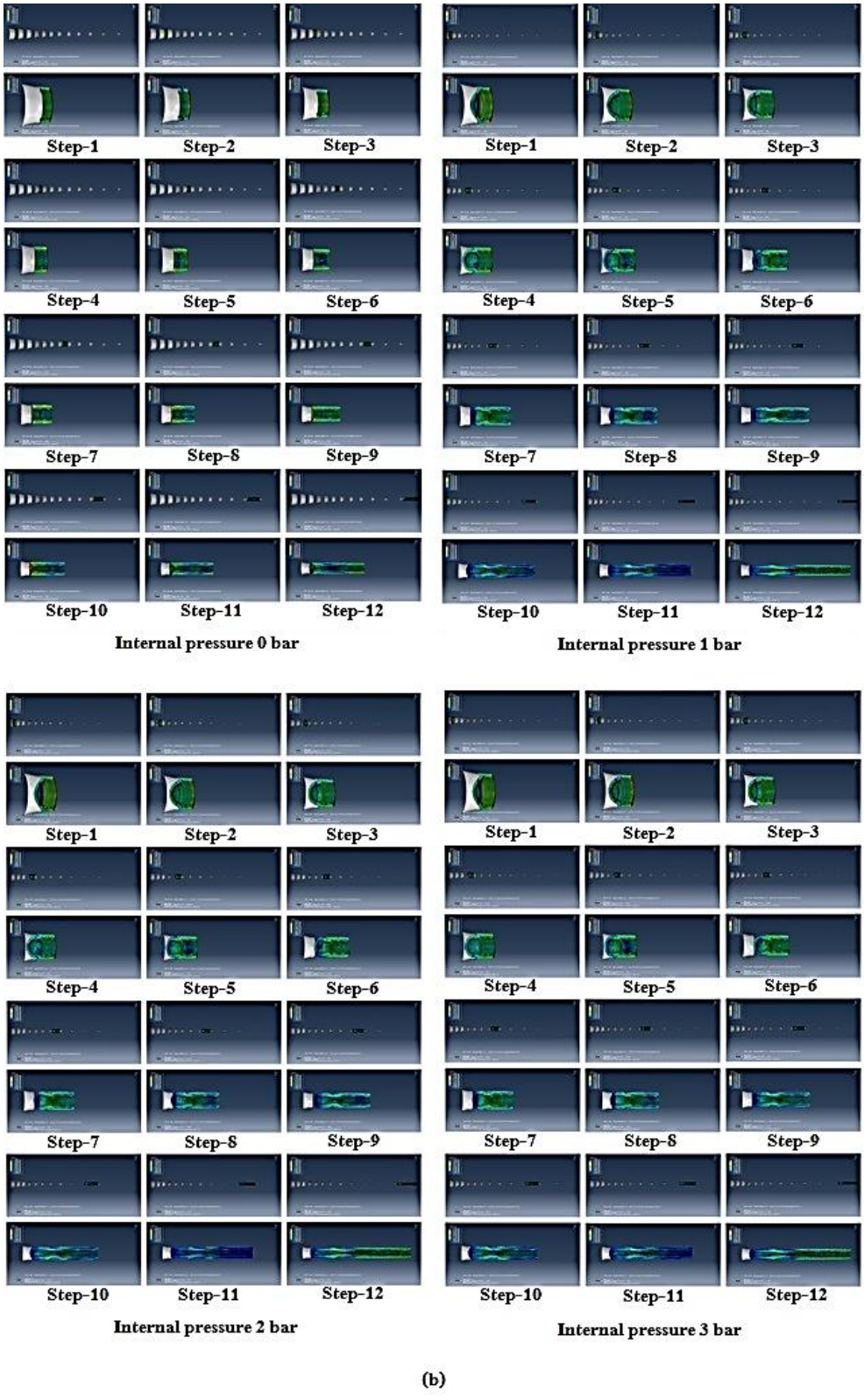

Figure 7 (a) Von Mises stress and FE simulation time (b) Distribution contour plot of equivalent von Mises stresses were different for various internal pressures inside the tubes before and after on the 1–12-step multi-pass process

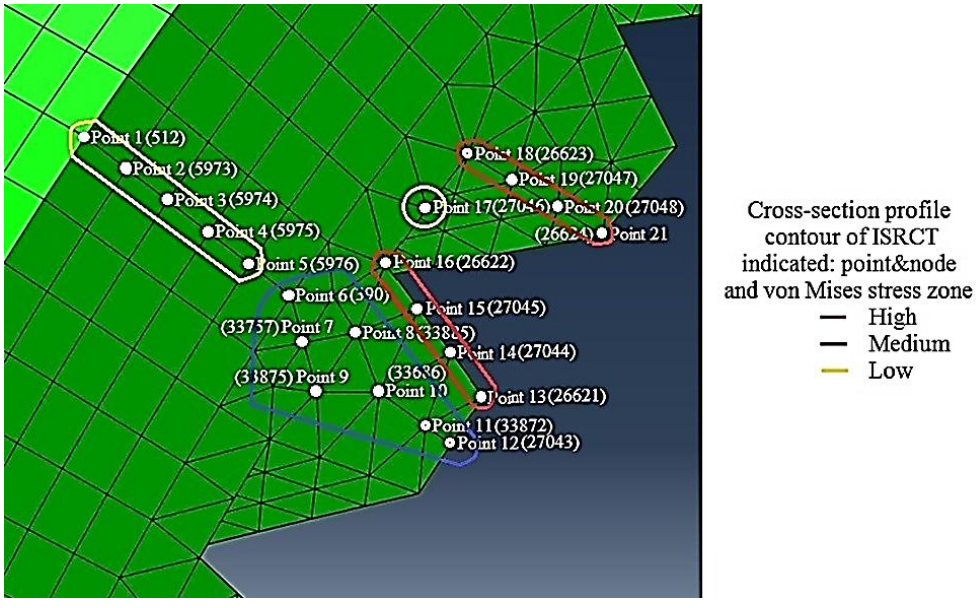

Figure 8 Cross-section profile of the ISRCT.

Figure 8 shows a cross-section profile contour of ISRCT to investigate von Mises stress simulations. The von Mises stress is often used in determining whether an isotropic and ductile metal will yield when subjected to a complex loading condition. The von Mises stresses simulations for various internal pressures inside the tubes are quite similar of each point. This was carried out to identify the best performed configuration at any point, i.e., point 1 (node 512), point 2 (node 5973), point 3 (node 5974), point 4 (node 5975), point 5 (node 5976), point 6 (node 390), point 7 (node 33757), point 8 (node 33885), point 9 (node 33875), point 10 (node 33686), point 11 (node 33872) and point 12 (node 27043), point 13 (node 26621), point 14 (node 27044), point 15 (node 27045), point 16 (node 26622), point 17 (node 27046), point 18 (node 26623), point 19 (node 27047), point 20 (node 27048) and point 21 (node 26624). The variations measured the existence of redundant von Mises stress, which occurred for various internal pressures inside the tubes as a result of the multi-pass tube drawing. Von Mises stress increased for all nodes after multi-pass drawing across the die. In this simulation, von Mises stress was highest from point 13, 14, 15, 16, 18, 19, 20 and 21 at the lateral edge of the ribbed regions, and medium at points 6, 7, 8, 9, 10, 11 and 12 at the ribbed regions. The trend was lowest on point 1, 2, 3, 4 and 5 at the wall thickness of the tube regions respectively.

In the drawing method, the behaviour of the copper tubes produced a spiral ribbed on the inside surface of the tube after drawing. The cross-sectional area and the ribbed spiral on the surface inside the tube changed after the deformation by drawing the different for various internal pressures inside the tubes. Results showed that the cross-sectional area of the spiral ribbed on the inside surface of the tube changed with drawing from the lowest R_t at 11.05 % to the highest with the R_t at 84.10 %, using simulation approach. The size of the cross-sectional dimension and the angle of the ribbed internal spiral changed after every multi-pass drawing and the thickness of the wall increased because of the outside diameter reduced while the tube itself took up

the compressive stress in one direction along the circumference of the tube. Finally, in the tube drawing method, the wall thickness of the ISRCT increased with the number of multi-pass drawings and the internal pressure 0 bar is unsuitable for drawing the inner spiral ribbed copper tubes. The relationship between wall thickness and FE simulation time is shown in Figure 9a.

In the FEM simulation results, the ribbed base width and ribbed tip width were possibly reduced due to the compressive strain in the circumferential direction. In case of the internal pressure 0 bar, the width of the ribbed base gradually reduced during the multi-stage tube drawing process. When D=1.64 mm (R_t = 77.36 %) at multi-pass drawing 10, the ribbed base widths contacted each other. On the contrary, the internal pressure 1, 2 and 3 bar, the pressure acted as the resistance pressure force inside the tubes. This was perpendicular to the inner surface of tube wall with pressure contact; the ribbed base width and ribbed tip width were expanded more than previously. The relationship between the ribbed base width and FE simulation time is shown in Figure 9b.

In case of inside the tube, when D=1.47 mm (R_t = 80.97 %) at multi-pass drawing 11, the ribbed tip widths contacted each other. In contrast, the changes were minimum if internal pressure 1, 2 and 3 bar respectively. The relationship between the ribbed tip width and FE simulation time is shown in Figure 9c.

The FEM simulation results show uneven deformation in several layers of the ISRCT. It is difficult to observe and clarify the deformation behaviour of inner gaps and the ribbed area during the internal pressure 0 bar inside the tube. In order to investigate the stress and strain, the effective strain distribution is similar to the effective stress. The strain reached maximum at the blending region between the gaps and the ribbed sections. The average strain in a gap region was larger than that in the ribbed areas. A gap deformation is therefore more intensive than that of a ribbed area. The gap of the ribbed area changed in a negative way. When D = 2.05 mm (R_t = 68.81%) at multi-pass drawing 8, the beginning of a flute mark was generated in the middle of the gap outside the ribbed section and a lug was generated on the back side of the flute mark. The folding gaps seldom generated at other places, except in the middle of the gap; their dimensions increased with further no pressure inside the tube drawing. Furthermore, several folding gaps appeared simultaneously around the circumference of the ribbed base line. Their dimensions were not all equal, and their distribution was not uniform over a circumference sector of the ribbed area. The relation between the ribbed base gap and FE simulation time is shown in Figure 9d.

Similarly, to the ribbed base gap, the strain on a ribbed tip gap reached maximum at the blending region between the gaps and ribbed areas. The average strain and gap deformation were more intensive than in a ribbed area. The gap of the ribbed section also changed in a negative way. In case of no pressure inside the tube, when D = 1.47 mm (R_t = 80.97 %) at multi-pass drawing 11, the gap vanished completely and no gaps were available except on the rough inner surface. When the internal pressure is increased to 1, 2 and 3 bar, respectively. The ribbed tip gap is rising as compared to the absence of internal pressure. Thus, values should be carefully designed in the multi-pass tube drawing process to manufacture ISRCT. The relationship between the ribbed tip gap and FE simulation time is shown in Figure 9e.

The simulation results for the total reduction area show a high deformation of the ribbed section. The internal pressure 0 bar inside the tube was no pressure resistance of elastic–plastic deformation with the multi-pass drawing of the ISRCT in the tube drawing method. As the outside diameters reduced, the compressive stress inside the ribbed region of the tube increased. Therefore, the direction along the circumference of the height of the ribbed area was compressed. The height of the ribbed is raised slightly due to the internal pressure acts at the lateral edge of the ribbed higher than the top of the ribbed. The relationship between the ribbed height and FE simulation time is shown in Figure 9f.

Figure 9g. shows the ribbed pitch reduced continuously as the outside diameter reduced to be consistent with the total reduction in size. The tube took up the compressive stress in the circumference of the ISRCT, which depended on the number of multi-pass drawings and the FE simulation time.

In case of no pressure inside the tube, when adaptive meshing was performed, a material point coincident with a node at the beginning of the step did not remain coincident with that node throughout the step. Values of displacement and current coordinates represent the motion of the node, not necessarily the motion of the material. This output provided the magnitude of the maximum displacement and the node and degree of freedom where the maximum displacement increment occurred during each multi-pass. In addition, the nodes which experienced changes in geometric features were 0.0511 mm in this case. When the internal pressure is increased to 1, 2 and 3 bar, the axial displacement changes were 0.0784, 0.0797 and 0.0798 mm respectively. The relationship between the axial displacement and FE simulation time is shown in Figure 9h.

The ribbed spiral angle decreased after 12 multi-pass drawings and this increased the total reduction area of the ISRCT. The size reduced because the axial displacement in the axial direction trended from the ribbed spiral angle. However, for a single rib, the strain distribution differed from the ribbed base to the ribbed tip. The strain at the ribbed base region and deformation were larger than those at the ribbed tip. The angle of the ribbed base and the ribbed tip changed in a negative way. Similarly, with simulation results, the ribbed spiral angle decreased and the angle of the ribbing approached 0 with time. However, the ribbed spiral angle decreased continuously over the same period, when the pressure inside ISRCT increased to 1, 2 and 3 bar, respectively. The spiral of the ribbed is raised slightly due to the internal pressure acts at the lateral edge of the ribbed higher than the top of the ribbed. The relationship between the ribbed spiral angle and FE simulation time is shown in Figure 10a.

Figure 10a. shows the results of FEM analysis for 1–12 multi-pass drawings. Figure 10b. in Table 2 summarized the results of comparing the characteristics and shows that the pressure inside ISRCT is increased 1, 2 and 3 bar, respectively. The internal pressure at 3 bar was the appropriate to fabrication of ISRCT in this case.

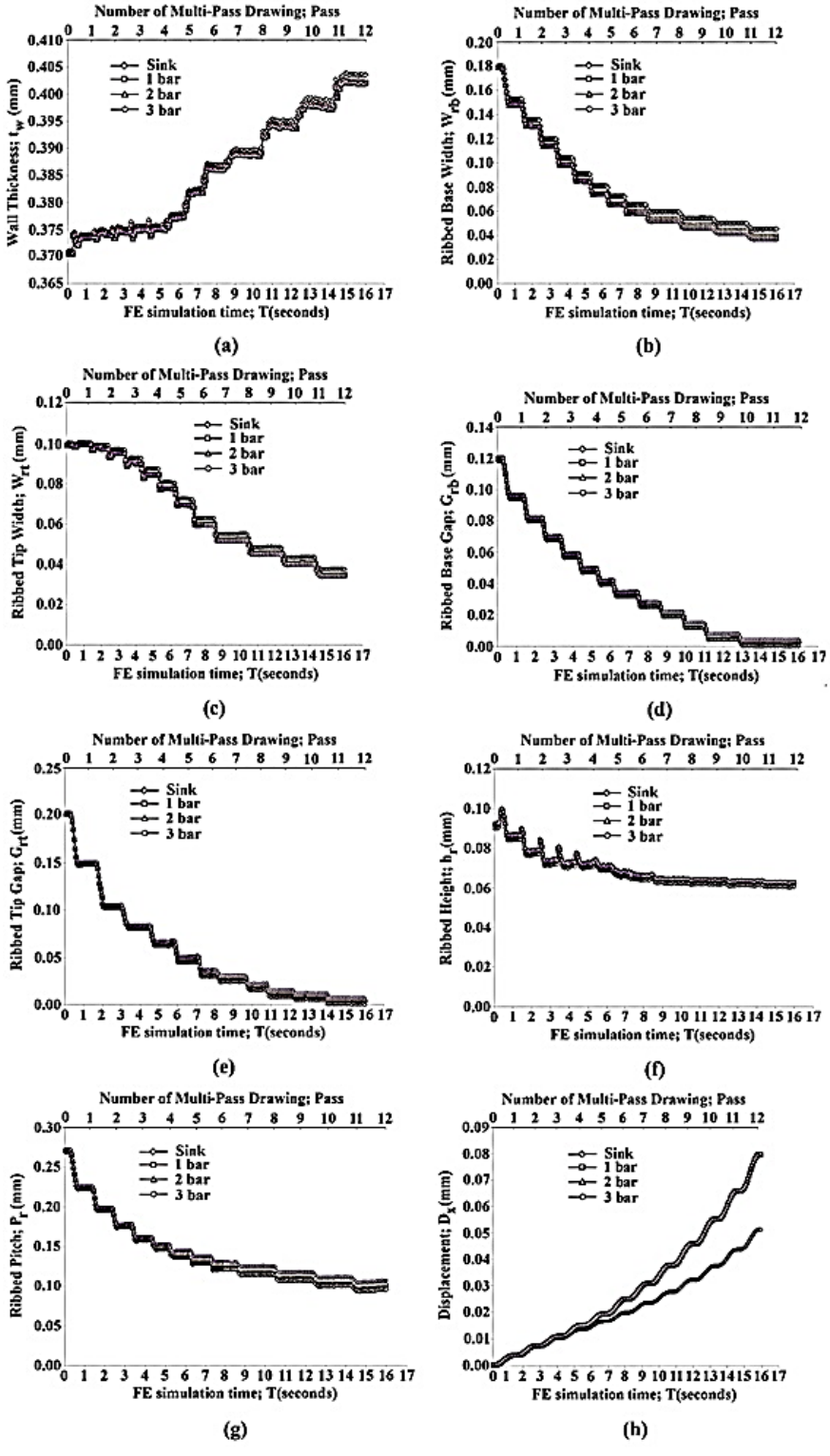

Figure 9 Summary of the results of the multi-pass drawing. **a** Wall thickness. **b** Ribbed base width. **c** Ribbed tip width. **d** Ribbed base gap. **e** Ribbed tip gap. **f** Ribbed height. **g** Ribbed pitch. **h** Axial displacement and FE simulation time

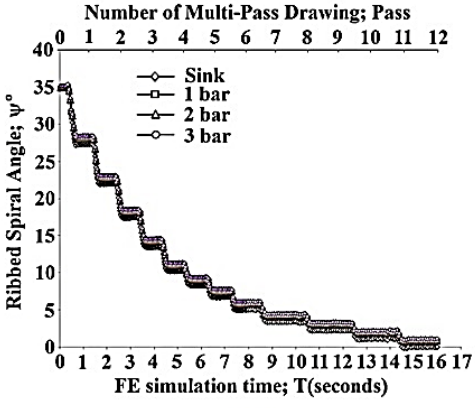

(a)

Table 2 Summary of the results comparing the characteristics

Parameter	Highest	High	Medium	Low
Von Mises stress	3 bar	2 bar	1 bar	0 bar
Wall thickness	0 bar	1 bar	2 bar	3 bar
Ribbed base width	0 bar	1 bar	2 bar	3 bar
Ribbed tip width	0 bar	1 bar	2 bar	3 bar
Ribbed base gap	3 bar	2 bar	1 bar	0 bar
Ribbed tip gap	3 bar	2 bar	1 bar	0 bar
Ribbed height	3 bar	2 bar	1 bar	0 bar
Ribbed pitch	3 bar	2 bar	1 bar	0 bar
Axial displacement	3 bar	2 bar	1 bar	0 bar
Ribbed spiral angle	3 bar	2 bar	1 bar	0 bar

(b)

Figure 10 Results of FEM analysis. **(a)** Ribbed spiral angle and FE simulation time. **(b)** Summary of the results comparing the characteristics

4. Conclusions

This paper is concerned with the development of ultra-small ISRCT with high-quality heat transfer using 3D FEM simulation study on effect of internal pressure and various pressures 0, 1, 2 and 3 bar, respectively. It was found that:

1. The influence of internal pressure on the ultra-small ISRCT, this process which arises from stress, including axial stress, radial stress and hoop stress. The stress increases in the ribbed wall and rapidly expands into the ribbed area regions. The von Mises stress after 12 multi-pass drawings was different for each locality. In this simulation, von Mises stress was highest at the lateral edge of the ribbed regions, the medium occurs at the ribbed regions, and the lowest on the wall thickness of the tube regions respectively. As a result, the von Mises stress on each node distribution is the same value as for four internal pressures (0, 1, 2 and 3 bar). The maximum stresses sorted according to the internal pressure of 3 bar, 2 bar, 1 bar and 0 bar, respectively.
2. While the expansion of effective strain was happened, the distributions of von Mises stress of ISRCT during the four inner pressures were increased after 12 multi-pass drawings. The changes of these parameters are as follows. Changes of cross-section profile on the horizontal and vertical axis of ISRCT using 3D FEM simulation was similar to the changes of the fluid mandrel drawing.
3. The results of the 3D FEM simulation were coincident with data from the fluid mandrel drawing. From the results, the internal pressure 0 bar (no pressure inside ISRCT) the changes of ribbed cross-sectional profile was similar to 1-3 multi-pass drawing of fluid mandrel drawing, and the internal pressure 1 bar the changes of ribbed cross-sectional profile was similar to 4-6 multi-pass drawing of fluid mandrel drawing, and the internal pressure 2 bar the changes of ribbed cross-sectional profile was similar to 7-9 multi-pass drawing of fluid mandrel drawing, and likewise the internal pressure 3 bar the changes of ribbed cross-sectional profile was similar to 10-12 multi-pass drawing of fluid mandrel drawing, respectively.

4. To summarise the analysis of the ten parameters, the cross-section profile distribution was the same value as varied internal pressures inside ISRCT, the effect of the ribbed spiral angle and the ribbed cross-sectional profile were similar compared to the fluid mandrel drawing. These results can be used to predict the final precision diameter of the ISRCT for fluid mandrel drawing and industrial manufacturing processes.

Acknowledgments

The authors would like to express deep appreciation to Prof Dr. Kazunari Yoshida, Department of Precision Engineering, Tokai University, 1117 Kitakaname, Hiratsuka, Kanagawa, Japan 259–1292, and Assoc. Prof Dr. Somchai Norasethasopon Department of Mechanical Engineering, Faculty of Engineering, King Mongkut's Institute of Technology Ladkrabang, Bangkok, Thailand for valuable and useful advice and comments.

References

[1] Tangsri T, Norasethasopon S, Yoshida K (2014) Fabrication of small size inner spiral ribbed copper tube by fluid mandrel drawing. Int J Adv Manuf Technol 70:1923–1930

[2] Tangsri T, Norasethasopon S (2013) Fabrication of small size inner spiral ribbed copper tube using tube sinking method. Adv Mater Res 802:37–41

[3] Tangsri T, Norasethasopon S (2013) Effects of rib dimension reduction and orientation change of inner spiral ribbed copper tube using tube sinking method. The 27th Conference of the Mechanical Engineering Network of Thailand: Pattaya, Chonburi

[4] Tangsri T, Norasethasopon S (2015) Influences of total reduction of area on drawing stress and tube dimension in inner spiral ribbed copper tube sinking. Int J Adv Manuf Technol 77:2269–2276

[5] Tangsri T, Norasethasopon S (2015) 3D FEM validation of ultra-small inner spiral ribbed copper tube using the tube sinking method. Int J Adv Manuf Technol 81: 1949–1959

[6] Dieter GE (1988) Mechanical metallurgy. SI metric edition, McGraw-Hill, ISBN 0-07 100406-8

[7] Sachs G, Baldwin WM (1946) 'Stress analysis of tube sinking', Trans. Am. Soc. mech. Engrs 68: 655–662